Journal of Power Sources 257 (2014) 174–180

Contents lists available at ScienceDirect

Journal of Power Sources

journal homepage: www.elsevier.com/locate/jpowsour

The electrochemical performances of Zn–Sn–Al-hydrotalcites in Zn–Ni secondary cells

Tingting Wang [a], Zhanhong Yang [a,b,*], Bin Yang [a], Ruijuan Wang [a], Jianhang Huang [a]

[a] College of Chemistry and Chemical Engineering, Central South University, Changsha 410083, China
[b] Key Laboratory of Resource Chemistry of Nonferrous Metals, Ministry of Education, Central South University, Changsha 410083, China

HIGHLIGHTS

- Zn–Sn–Al-hydrotalcites with layered structure was prepared and proposed as zinc electrode material for the first time.
- The special structure has attributed to the electrochemical performances of zinc electrode with Zn–Sn–Al-hydrotalcites.
- Zinc electrode with Zn–Sn–Al-hydrotalcites shows superior electrochemical cycle stability.

ARTICLE INFO

Article history:
Received 30 November 2013
Received in revised form
19 January 2014
Accepted 1 February 2014
Available online 11 February 2014

Keywords:
Zinc–nickel secondary cells
Zn–Sn–Al-hydrotalcites
Electrochemical behavior
Cyclic voltammograms

ABSTRACT

Zn–Sn–Al-hydrotalcites (LDHs) have been successfully prepared by hydrothermal method and applied as a novel anodic active material in Zn–Ni secondary batteries. The scanning electron microscopy (SEM), X-ray diffractometer (XRD) and FT-IR tests are performed to investigate the morphology and microstructure of Zn–Sn–Al-hydrotalcites. Electrochemical performances of Zn–Sn–Al-hydrotalcites with different Zn/Sn/Al molar ratios are investigated through galvanostatic charge–discharge measurements, cyclic voltammograms (CV) and Tafel polarization curves. Compared with Zn–Al–LDH without Sn addition, Zn–Sn–Al–LDHs still present hexagon layer structure, and present more excellent electrochemical performance. And Zn–Sn–Al–LDH with the molar ratio of 2.8:0.2:1 shows a better cycle stability than the other samples. The results demonstrate that Sn addition can help to perfect the electrochemical performance of zinc electrode with Zn–Sn–Al–LDHs. At the same time, CV tests indicate well reversibility and Tafel curves reveal more positive corrosion potential for Zn–Sn–Al–LDHs.

1. Introduction

It's well known that Zn–Ni alkaline secondary system is a promising candidate for green power sources used in hybrid/electric vehicles and have attracted a rising attention in recent years. This system exhibits good performance: long cycle life of nickel anode and high capacity of zinc cathode [1–5]. In addition, the zinc electrodes have many excellent properties such as high specific energy density and specific power, high open circuit voltage, low toxicity and low cost [6,7]. However, the industrialization of Zn–Ni alkaline secondary batteries is impeded severely for some drawbacks of zinc electrodes: poor cycle life, the shape change, dendrite growth, surface passivation, zinc self-corrosion and self discharge, which are resulted from a high solubility of zinc discharge products and the non-uniform deposition of zinc active material during charging [8–10]. Hence, many efforts have been devoted to conquer these problems, including additives to the anode and the electrolytes, development and improvement of separators, miscellaneous techniques such as pulse charging, electrode vibration and surface modification technique to improve the electrochemical performance of ZnO [11–20]. It's necessary to find a better and novel anode material to address these problems.

Layered double hydroxides (LDHs), as a class of anionic exchange layered material, have attracted a lot of research and have been applied in many fields. As we know, the layered double hydroxides (LDHs) or hydrotalcite similar to LDHs has a formula of $[M(II)_{1-x}M(III)_x(OH)_2]^{x+}[(A^{n-})_{x/n}\cdot MH_2O]^{x-}$, where M(II) represents any divalent metal cation, M(III) trivalent metal cation, and A^{n-} an anion, whose structure is similar to that of brucite ($Mg(OH)_2$). The studies published in the past decades, showed that the partial replacement of the cations in the layers with two or three divalent or trivalent transition metal cations with redox properties that have

* Corresponding author. Tel./fax: +86 0731 88879616.
E-mail addresses: zhyang@mail.csu.edu.cn, zhongnan320@gmail.com (Z. Yang).

http://dx.doi.org/10.1016/j.jpowsour.2014.02.006
0378-7753/

an ionic radius similar to Mg^{2+} or Al^{3+}, can produce different functional performance in favor of practical applications [21–24]. The special layered LDHs have been widely applied in fields of catalysts, nanofillers, drug delivery material and chemically tailored functional material [25–27]. Because of their alkalescence, layered structure and stability in alkaline solution, LDHs may be an important component of electrode material for alkaline batteries. However, the electrochemical properties of LDHs for secondary cells have been attracted only a few attentions. Zn–Al–LDHs introduced as novel anodic material in Zn–Ni secondary cells have been investigated and delivers a high initial discharge capacity [28,29]. But pure Zn–Al–LDHs as anodic material suffer low conductivity. Therefore, it's necessary to modify it to perfect the electrochemical performance. The effect of partial replacement of trivalent transition metal cation (La^{3+}) on the electrochemical performance was studied by Fan and revealed that the presence of La^{3+} can help to improve the corrosion potential [30]. Wang [31] have revealed that a partial replacement of Al by In is in favor of better electrochemical performance. In this work, we emphasis on the partial replacement of divalent metal cation and proposed a novel zinc electrode material of Zn–Sn–Al–LDHs for the first time and the electrochemical properties were studied in details.

2. Experimental

2.1. The preparation of Zn–Sn–Al-hydrotalcites

Zn–Sn–Al–LDHs were prepared by the method of hydrothermal. The typical experimental operation was as follows: Zinc, Aluminum nitrates (AR, Tianjin City Guang Fu Fine Chemical Institute) were dissolved in a certain volume of deionized water, Stannous chloride (AR, Shanghai City Jin Shan Ting Xin Chemical Institute) was dissolved in concentrated hydrochloric acid solution, keeping the Zn/Sn/Al molar ratio of 3:0:1, 2.9:0.1:1, 2.8:0.2:1 and 2.7:0.3:1; then the above two saline solution and a mixture containing NaOH (2 mol L^{-1}) and Na_2CO_3 (0.5 mol L^{-1}) (AR, Tianjin City Guang Fu Fine Chemical Institute) were added simultaneously to a three-necked flask at a speed of 1 drop s^{-1}, keeping the total metal ion concentration of 1.0 mol dm^{-1}, which contained 100 ml deionized water and was under the protection of inert gas nitrogen. The process was carried out under vigorous stirring at 40 °C, and appropriate amount of NaOH solution was added to keep the pH value of 10. After stirring for 30 min, the mixture was poured into Teflon-lined autoclave, and then kept for 10 h under 120 °C. The product cooled to room temperature was filtered and washed for several times with deionized water and ethyl alcohol until the pH reached 7, dried for 24 h under 60 °C and ground to fine powder.

2.2. The characterizations of Zn–Sn–Al-hydrotalcites

Fourier transform infrared (FT-IR) spectroscopy was carried out on a Nicolet Nexus-670 FT-IR spectrometer (as KBr discs, with wave number 400–4000 cm^{-1}, resolution 0.09 cm^{-1}, and the weight of measured sample 2 mg). X-ray diffraction (XRD) was performed on a D500 (Siemens) diffractometer (36 KV, 30 mA) using Cu Kα radiation at a scanning rate of $2\theta = 8^\circ$ min^{-1}. The morphology of as-synthesized Zn–Sn–Al–LDHs (with the Zn/Sn/Al molar ratio of 2.8:0.2:1) was observed using scanning electron microscope (SEM, JSM-6360LV).

2.3. The preparation of Zn–Sn–Al–LDHs electrodes

The Zn–Sn–Al–LDHs electrodes were prepared by incorporating slurries containing Zn–Sn–Al–LDHs, acetylene black and Polytetrafluoroethylene (PTFE, in diluted emulsion) to a copper mesh substrate (1.0 cm × 1.0 cm in size). The weight ratio of Zn–Sn–Al–LDHs, acetylene black, and PTFE was 80:10:10. The obtained zinc electrodes were pressed to a thickness of 0.20 mm and dried at 80 °C under vacuum. Zn–Al–LDH electrodes composed of Zn–Al–LDHs were also fabricated through the same way for comparison. A two-electrode cell was assembled for pre-activated testing of cell. A solution of 6 mol dm^{-3} KOH with saturated ZnO was used as the electrolyte. The polypropylene micro-porous membrane was used as the separator. The sintered Nickel electrodes were used as positive electrodes, whose capacity was much more than that of the zinc electrodes prepared for the purpose of full use of Zn–Al–LDHs material during cycling. All the electrodes were pre-activated for 6–8 times through the steps: charged at constant current of 0.1 C for 600 min, and discharged at constant current of 0.2 C to a cut-off voltage of 1.4 V at room temperature.

2.4. The measurements of electrochemical properties

The galvanostatic charge–discharge tests were carried out on a BTS-5 V/20 mA battery-testing instrument (Neware, China) at room temperature. A two-electrode cell system was assembled for cyclic testing with a counter electrode of sintered Nickel electrode. During cycling process, the cells were charged at 1 C for 60 min and discharge at 1 C down to a 1.4 V cut-off voltage. A three-electrode cell was assembled for cyclic voltammograms (CV) and Tafel polarization, with Hg/HgO electrode served as reference electrode, pre-activated zinc electrode as working electrode and the sintered Nickel electrode as counter electrode. The capacity of counter electrode was far higher than that of zinc electrode. The electrolyte was 6 mol dm^{-3} KOH solution with saturated ZnO. The CV test was carried out on an electrochemical workstation (CHI660B) at room temperature at a scanning rate of 5 mV s^{-1} ranging from −0.80 V to −1.65 V. Tafel polarization curves were also performed using an electrochemical workstation (CHI660B) at room temperature at a scanning rate of 0.5 mV s^{-1}.

The reagents used in all the above experiments were A.R. grade and the electrolyte was prepared with deionized water.

3. Results and discussions

3.1. Structural analysis of Zn–Sn–Al–LDHs

The typical FT-IR spectra of Zn–Al–LDH and Zn–Sn–Al–LDH are depicted in Fig. 1. The broad peak at 3441.27 cm^{-1} can be described to the stretching of OH^- groups attached to metal ions. The bending vibration of interlayer water appears at 1509 cm^{-1}, which is shifted to lower direction slightly compared with liquid water at about 1600 cm^{-1}. A considerably lower shifted absorption peak at 1362 cm^{-1}, compared with CO_3^{2-} of $CaCO_3$ at 1430 cm^{-1}, shows that there is an intercalation between CO_3^{2-} and interlayer H_2O through the strong hydrogen bonding. The bands around 650-500 cm^{-1} are attributed to Zn–O. The absorption peaks at 552.1 cm^{-1} and 786.9 cm^{-1} present the Al–O stretching modes and Sn–O appears at 427.56 cm^{-1}.

Fig. 2 shows the XRD pattern of the as-prepared Zn–Al–LDH (coded A) and Zn–Sn–Al–LDH (coded C, with molar ratio of 2.8:0.2:1) powder, as comparison. It can be seen clearly that the strong and sharp diffraction peaks of Zn–Sn–Al–LDH at $2\theta = 11.684^\circ$, 23.441°, 34.572°, 61.526° are corresponding to the relation of (003), (006), (009) and (110) accordingly, which can also be seen in that of Zn–Al–LDH. The sharp, narrow and symmetrical diffraction peaks indicate a well-crystallized sample with a low and stable baseline. The highest diffraction peak appeared at $2\theta = 11.684^\circ$ suggests that the hydrotalcite-like compound Zn–Sn–

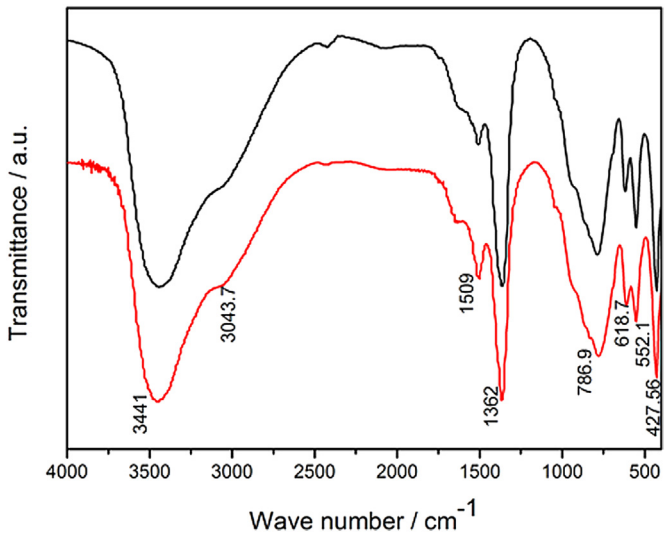

Fig. 1. FT-IR curves for Zn–Al–LDH and Zn–Sn–Al–LDH (with Zn/Sn/Al = 2.8:0.2:1) samples.

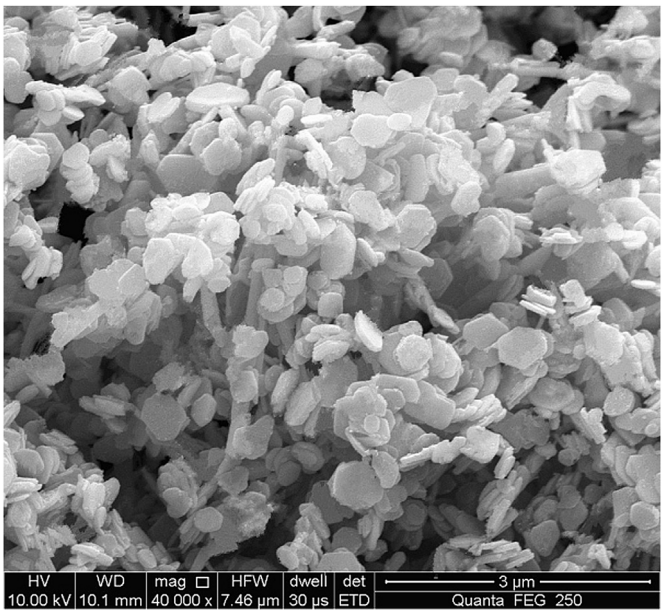

Fig. 3. SEM images for Zn–Sn–Al–LDH (with Zn/Sn/Al = 2.8:0.2:1) sample.

Al–LDH is highly crystallized and has a typical hexagonal crystal structure.

The typical SEM image of Zn–Sn–Al–LDH is presented in Fig. 3. The basic morphology of hydrotalcite with Sn addition steel keeps lamellar, which is the typical structure of Zn–Al–LDH [29]. This result shows that appropriate addition of Sn do not destroy the lattice structure of active material [30–32]. The particle size is about 160–250 nm. Based on the analysis above, Zn–Sn–Al–LDH is produced successfully through hydrothermal method.

3.2. The galvanostatic charge/discharge curves analysis of zinc electrodes

Fig. 4 presents the typical galvanostatic charge/discharge curves of zinc electrode with Zn–Sn–Al–LDHs tested at 20th cycle. The batteries with Zn:Sn:Al = 3:0:1, 2.9:0.1:1, 2.8:0.2:1 and 2.7:0.3:1 are coded A, B, C and D respectively. As shown in Fig. 4, the cells with sample B, C and D show lower charge plateau voltage and higher discharge plateau voltage compared with that of sample A. Especially, the cell with sample C (2.8:0.2:1) shows the lowest charge plateau voltage and highest discharge plateau voltage. In alkaline solution, the standard electrode potential of $Sn(OH)_3^-/Sn$ is larger than that of $Zn(OH)_4^{2-}/Zn$:

$$Sn(OH)_3^- + 2e \rightarrow Sn + 3OH^- \quad E^{\Theta} = -0.909\ V \tag{1}$$

$$Zn(OH)_4^{2-} + 2e \rightarrow Zn + 4OH^- \quad E^{\Theta} = -1.199\ V \tag{2}$$

In the process of activating, Sn^{2+} is inclined to be reduced to Sn metal [30]. The uniformly distributed Sn in the lamellar can help to increase the contact of active material with current collector and electrolyte. Sn metal can not be oxidized to Sn^{2+} again in the cycle process. Further more, Al^{3+} can not be reduced to Al, and exists steadily in zinc electrode, providing a stable framework of layered structure. When Sn^{2+} is reduced to Sn, Sn metal can stick to the framework, and form a conductive system in the lamellar as depicted in Fig. 5, the conductive network helps to improve the electronic transmission, decreasing the internal resistance of zinc

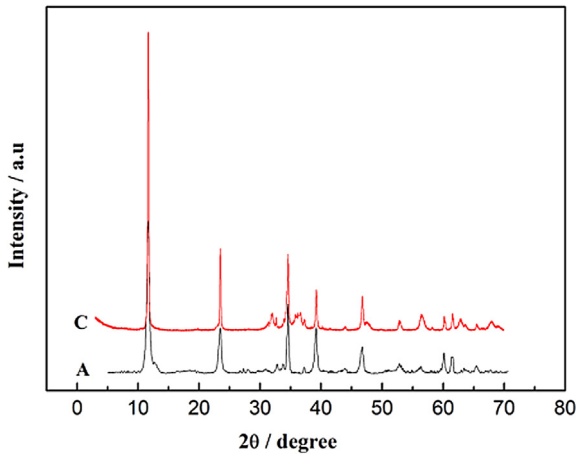

Fig. 2. XRD patterns of Zn–Al–LDH and Zn–Sn–Al–LDH (with Zn/Sn/Al = 2.8:0.2:1) samples.

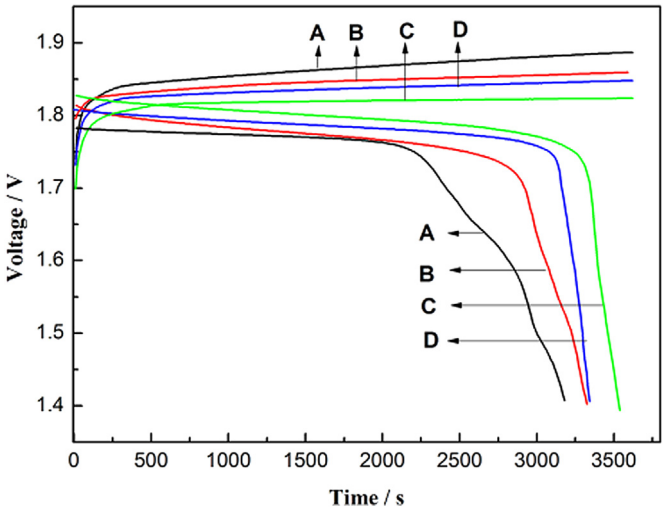

Fig. 4. Typical galvanostatic charge–discharge curves of Ni–Zn secondary batteries with Zn–Al–LDH and Zn–Sn–Al–LDH.

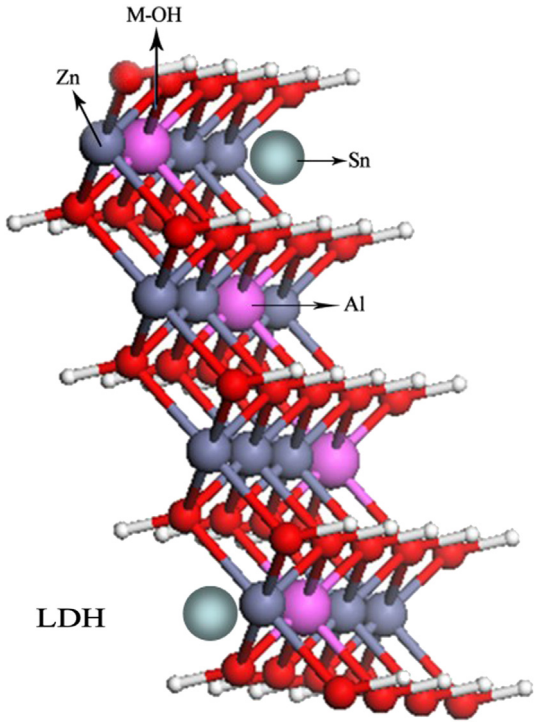

Fig. 5. The schematic diagram of Zn–Sn–Al–LDH after cycles.

electrode. And the distribution of current is more uniform compared with electrode A without Sn addition. This all means that a certain amount of Sn addition can help to improve the conductivity of zinc electrode. In consequence, the process of charge and discharge with electrodes B, C and D is easier than that of A, and electrodes with Sn addition present higher discharge platform and lower charge platform. In addition, electrode C with Zn/Sn/Al molar ratio of 2.8:0.2:1 shows the lowest charge platform compared with sample B and D. This is owing to that sample B with Zn:Sn = 2.9:0.1 has the smallest Sn ratio, which can not so obviously improve the internal resistance. And sample D with excessive Sn molar ratio can affect the regular layer structure of hydrotalcite, resulted from the larger atomic radius of Sn. The atomic radius of Sn is 0.112 nm, which is larger than that of Al (0.0535 nm) and Zn (0.074 nm). The excessive amount of Sn addition can leads to the disproportion of lattice, impacting the electrochemical performance of electrode D. As a consequence, Zn–Sn–Al–LDH with a molar ratio of 2.8:0.2:1 has the most excellent performance as a novel anode material. In order to account for this point, Fig. 6 shows the variation of internal resistance. As shown, electrode B, C and D show lower internal resistance compared with electrode A, and the electrode C with sample 2.8:0.2:1 shows the lowest internal resistance, which is in accordance with the results analyzed above. This also proves that the explanation is reasonable.

Fig. 7 shows the variation of midpoint discharge voltage versus cycle number of the batteries. Midpoint discharge voltage is an important parameter for rechargeable. Higher midpoint discharge voltage associates with higher discharge potential and better performance in discharge process [33]. As can be seen in Fig. 7 the midpoint discharge voltage of electrode B, C and D is higher compared with that of electrode A. And the midpoint discharge voltage stabilization of electrodes with Sn addition is better. It is the reason that Sn addition exists in the form of Sn metal and distributed uniformly in zinc electrode as explain above, cause the decrease of internal resistance. And electrode C with Zn/Sn/Al

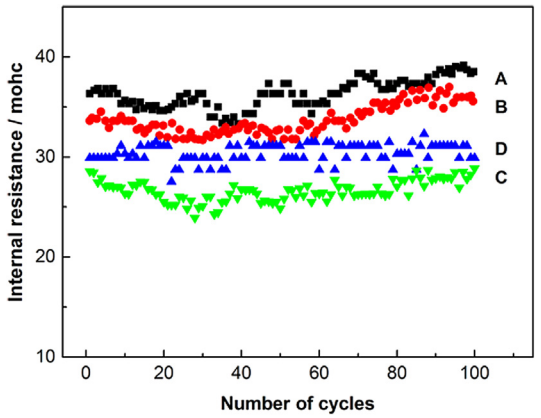

Fig. 6. The variation of internal resistance of electrodes with Zn–Al–LDH and Zn–Sn–Al–LDH samples.

molar ratio of 2.8:0.2:1 has the best midpoint discharge voltage performance, which is in accordance with the charge–discharge curves.

3.3. The cycle performance analysis of Zn–Sn–Al–LDHs electrodes

The discharge capacity of zinc electrodes with Zn–Sn–Al–LDHs is illustrated in Fig. 8 (a is the discharge capacity before 50 cycles; b is the discharge capacity from 50th cycle to 500th cycle). It can be found in Fig. 8a, the capacity of electrodes A, B, C and D is lower in the first several cycles because of the incomplete activation of active material. With the increase of cycling, active material is activated more and more completely. And it is clear that the discharge capacity of the four electrodes is promoted. As can be seen, the discharge capacity of electrode A decreases rapidly after 30th cycles. For comparison, electrodes B, C and D show more excellent cycle stability in the 50th cycles. Even when cycle number is increased to 500 as shown in Fig. 8b, the electrode D also keeps excellent cycle stability. This is resulted from the Sn addition. As mentioned above, Sn^{2+} can be reduced to Sn metal during the activating process, forming a conductivity network in the layered structure, the conductivity of zinc electrode can be enhanced, the current distribution in the electrode internal is more uniform than the electrode without Sn, improving the utilization of active material, resulting to the relatively higher discharge capacity of

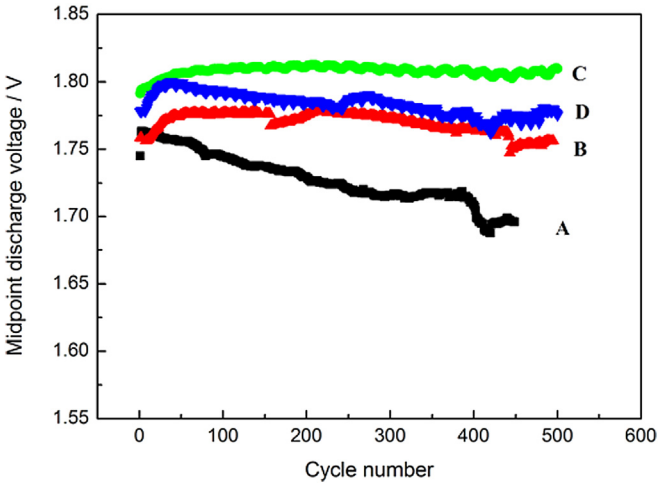

Fig. 7. The midpoint discharge voltage curves for Zn–Al–LDH and Zn–Sn–Al–LDH.

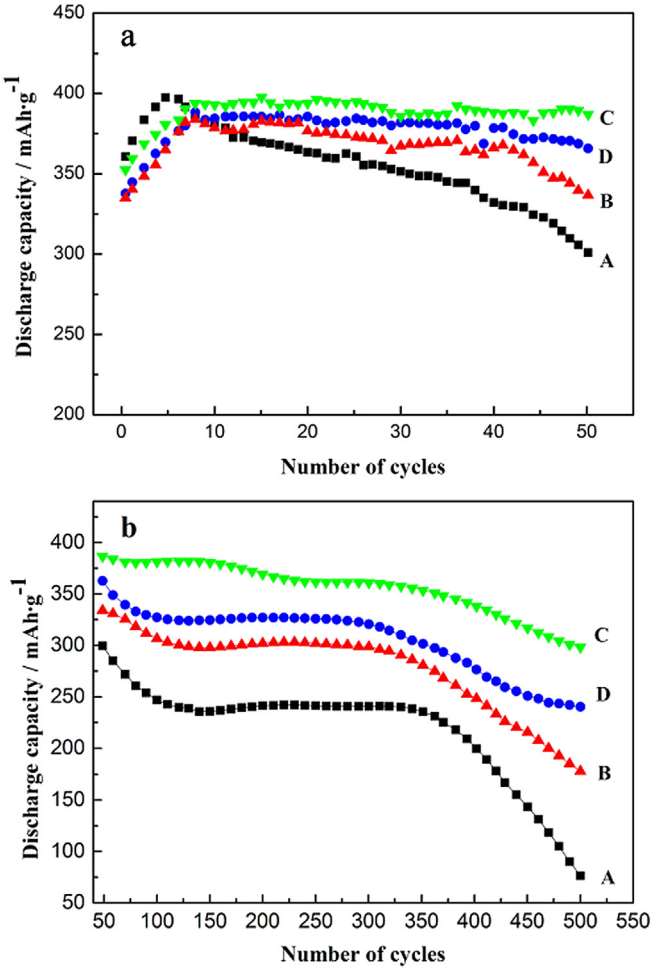

Fig. 8. The variation of discharge capacity with number of cycles for electrodes with Zn–Al–LDH and Zn–Sn–Al–LDH samples.

electrode B, C and D. For another, in the process of charging, reduced Sn metal can provide deposition point for the growth of Zn. The distribution of reduced Zn is more uniform, which can contribute to keeping the lamellar structure during cycle process. The stably maintained LDH structure also helps to prevent the shape change and suppress the dendrite growth of active material [30,31]. In order to further study the cycle life of battery with Zn–Sn–Al–LDH, the charge–discharge efficiency curves with cycles of electrodes B, C and D are presented in Fig. 9. The charge–discharge efficiency of electrode C is the highest compared with the other electrodes in the following 500 cycles. This phenomenon can be explained as that less amount of Sn addition as electrode B is not so effective to affect the electrochemical performance, but excessive Sn as electrode D will destroy the layered structure because of the larger atomic radius and prevent the improvement of electrochemical performance. A certain amount of Sn addition is important for the improvement of electrochemical performance, which is also mentioned above.

3.4. The Tafel plot curves analysis of zinc electrode

To understand the effects of Sn addition on polarization and corrosion behaviors of zinc electrodes, Tafel plot curves were carried out and the curves are shown in Fig. 10 with Zn:Sn:Al = 3:0:1(coded A), 2.9:0.1:1(coded B), 2.8:0.2:1(coded C), 2.7:0.3:1(coded D). Table 1 shows the electrochemical kinetic

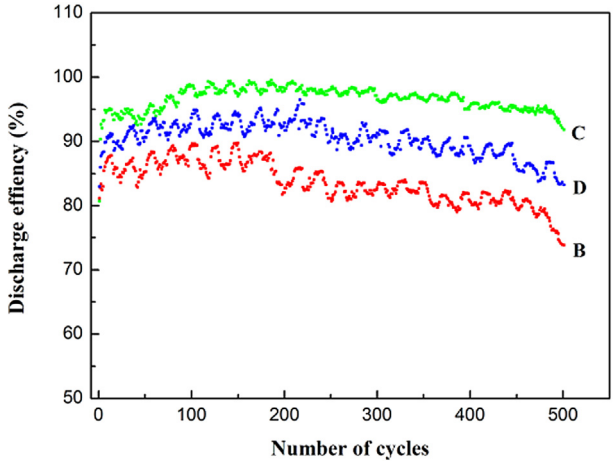

Fig. 9. The variation of discharge efficiency with number of cycles for electrode with Zn–Al–LDH and Zn–Sn–Al–LDH samples.

parameters derive from the curves, including corrosion potential (E_{corr}), corrosion current density (j_{corr}) and inhibition efficiency (j.E. %). The E_{corr} and j_{corr} are calculated through fitting linear equations to the logarithmic plots of current density as a function of potential [34]. The inhibition efficiency is calculated through the formula [30]:

$$\text{j.E.\%} = \left(j^0_{corr} - j_{corr}\right) \Big/ j^0_{corr} \times 100 \quad (3)$$

j^0_{corr} and j_{corr} present the corrosion current densities of electrode A without Sn and electrodes (B,C,D) with Sn addition. Apparently, the corrosion potential (E_{corr}) of zinc electrodes with Sn addition are shifted positively in varying degree compared with Zn–Al–LDHs electrode: the E_{corr} of sample A, B, C and D appear respectively at −1.3799 V, −1.3549 V, −1.3226 V and −1.3404 V. The j_{corr} of zinc electrodes with Sn addition are smaller obviously compared with electrode A as shown in Table 1. Especially, it can be seen from Table 1 that Zn–Sn–Al–LDH with Zn:Sn:Al = 2.8:0.2:1 presents the lowest corrosion current, and as a result the highest inhibition efficiency. As explained in the Principles of Electrochemistry of Corrosion, E_{corr} is the critical value the corrosion occurs on electrode, and more negative E_{corr} means the larger degree of corrosion. The j_{corr} means the corrosion speed, and smaller j_{corr} means the

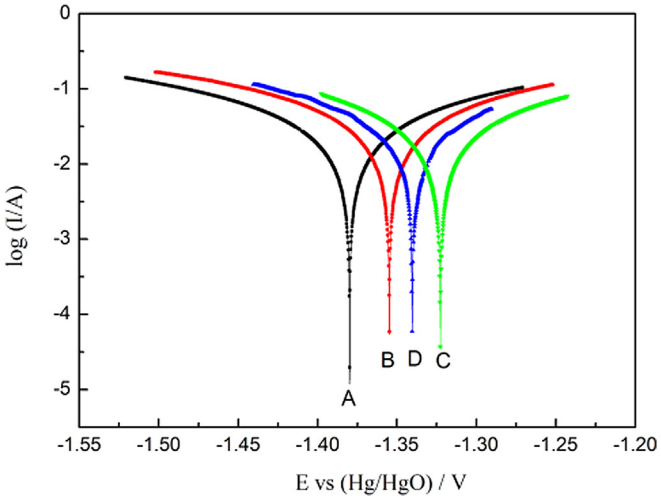

Fig. 10. Tafel plot curves for Zn–Al–LDH and Zn–Sn–Al–LDH samples.

Table 1
The dates for Tafel curves with Zn–Al–LDH and Zn–Sn–Al–LDH samples.

Sample	E_{corr} (V)	j_{corr} (mA cm^{-2})	j.E.%
A	−1.3799	3.98×10^{-2}	–
B	−1.3549	3.16×10^{-2}	20.6
C	−1.3226	1.26×10^{-2}	68.34
D	−1.3404	1.99×10^{-2}	50

better anti-corrosion property. The relation between j_{corr} and electrode potential can be depicted as:

$$j_{corr} = j_{o,c} \exp\left(\frac{E_{e,c} - E_{e,a}}{\beta_a + \beta_b}\right) \quad (4)$$

In case of other parameters are same or similar, the value of $E_{e,c} - E_{e,a}$ decreases as the decrease of j_{corr}. And the larger the value of $E_{e,c} - E_{e,a}$, the grater the corrosion rate is. So the decreased j_{corr} cause the improvement of anti-corrosion property. All the information implies that the anti-corrosion property of zinc electrodes with Zn–Sn–Al–LDH can be improved owing to the presence of Sn addition. Because of the relatively higher hydrogen evolution overpotential, the electrode polarization will decrease with the increase of Sn addition, causing the positively shifted E_{corr}. But excessive Sn addition will destroy the regular structure, and the internal resistance increase, resulting to the increase of electrode polarization. The result agrees with that of internal resistance, and the analysis is in accordance with experiment result. So a certain amount of Sn addition with higher corrosion potential can help to decrease the electrode polarization during work process [32,35], and electrode corrosion is inhibited in alkaline electrolyte.

3.5. The cyclic voltammogram (CV) analysis of zinc electrodes

In order to further study on the electrochemical reactions of Zn–Sn–Al–LDH during the charge–discharge cycles, cyclic voltammogram (CV) tests at 20th cycle are performed and the results are shown in Fig. 11. The current response appeared between −0.9 V and −1.65 V. The zinc electrodes with Zn:Sn:Al = 3:0:1, 2.9:0.1:1, 2.8:0.2:1 and 2.7:0.3:1 are coded A, B, C and D respectively. As can be seen, in cathode area, the peak potential of electrode A appears at −1.501 V, and electrode B, C and D at −1.492 V and −1.477 V, −1.484 V. Generally speaking, a more negative potential, means a lower electrochemical kinetics of reduction process, that is to say, electrode B, C and D shows better electrochemical kinetics, and the charging process is more effective and rapid [4]. The cathode process reflects the charge process of Zn–Ni secondary battery, more positive peak potential means the lower charge platform voltage [36], which is in corresponding with the charging process showed in Fig. 4. And in the anodic area, electrode A appears anode peak firstly at −1.139 V. The anodic peaks of zinc electrodes with sample B, C and D appear at −1.194 V, −1.271 V, and −1.245 V. It is obvious that anode peak potential of electrodes B, C and D is lower relatively than that of electrode A. The negatively shifted anode peak potential of electrode with Sn addition can be explain by the effect of Sn. The presence of reduced Sn helps to form conductive network, improving the conductivity in layered structure, the electronic conductivity is increased [32]. So the anode reaction can occur at lower potential. Especially, sample C with Zn:Sn:Al = 2.8:0.2:1 shows the lowest anode peak potential compared with that of sample of A, B and D. The reason is that as the amount of Sn addition increasing, the conductivity caused by the conductive network is becoming better, but excessive Sn addition will destroy the layered structure, resulting to the decrease in electrochemical performance. The anodic process reflects the discharge process of Zn–Ni secondary battery. The lower anode peak potential means the higher electrochemical activity of zinc electrode, and discharge process can occur in lower potential, resulting to the higher discharge platform voltage. The result is in accordance with the galvanostatic charge–discharge curves showed above. Further more, the difference between cathode peak and anode peak potential of electrode C (Zn:Sn:Al = 2.8:0.2:1) is small. The smaller the difference between anode and cathode potential, the better the reversibility of electrode is [19]. So electrode C has the best reversibility. A certain amount of Sn addition is in favor of improving the electrode efficiency and reversibility [37].

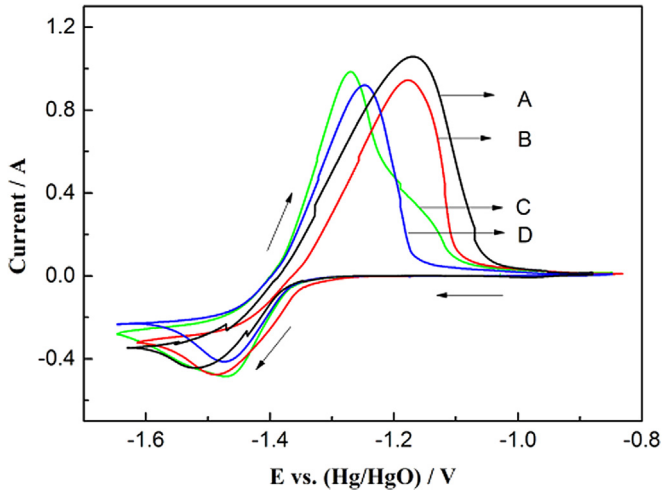

Fig. 11. Cyclic voltammograms curves of Zn–Al–LDH and Zn–Sn–Al–LDH samples.

As for the larger anodic oxidation peak compared with the cathode peak, we can explain it from the Randles–Sercik equation:

$$I_p = 0.4463nFAC^0v^{1/2}\sqrt{\frac{nFD}{RT}}$$

where n means the charge transfer number during redox reaction; A depicts the area of electrode; C is the concentration of the reactants; v is the scanning speed of CV test; and D means the diffusion coefficient.

In the equation, n and FA, v, D, R, T are constant. So the I_p is related to C. In the cathode area, the $Zn^{2-} + 2e \rightarrow Zn$ reaction occurs; and in the anode area, $Zn - 2e \rightarrow Zn^{2-}$ reaction occurs. In the cathode area, Zn^{2-} exists in the special layered structure of LDH, the concentration of Zn^{2-} is small, but in the anode area, the concentration of the reactants is 1 (reactant is Zn metal), so the I_p of anode peak is larger than that of cathode peak, resulting to the larger anode peak. Many studies have shown that the CV tests have the similar curve characteristics [10,11,15,19,38].

4. Conclusion

Zn–Sn–Al–LDH prepared by hydrothermal method remains the hexagon layer structure, and shows better electrochemical performances compared with Zn–Al–LDH as anodic active material. The corrosion potential of Zn–Sn–Al–LDH with different Zn/Sn/Al molar ratio, especially with the sample of Zn/Sn (2.8:0.2), is more positive, and exhibits better reversibility in CV test and superior electrochemical cycle stability in galvanostatic charge/discharge process. The utilization ratio of active material is promoted owing to the Sn addition. CV test reveals a better reversibility of zinc electrode with sample of Zn/Sn (2.8:0.2). All the investigation results make sure that Zn–Sn–Al–LDH is a novel anode active

material with good electrochemical performances in Zn–Ni secondary battery.

Acknowledgments

This work was financially supported by the Natural Science Foundation of China (no. 21371180 and 91023031), Doctoral Fund of Ministry of Education of China (20130162110 018) and the Science and Technology Project of Changsha City (No. k1303015-11 and k1203014-11).

References

[1] Z.Y. Tan, Z.H. Yang, X. Ni, H.Y. Chen, R.J. Wen, Electrochim. Acta 85 (2012) 554–559.
[2] H. Chang, C. Lim, J. Power Sources 66 (1997) 115–119.
[3] S.H. Lee, C.W. Yi, K. Kim, J. Phys. Chem. C 115 (2011) 2572–2577.
[4] M. Ma, J.P. Tu, Y.F. Yuan, X.L. Wang, K.F. Li, F. Mao, Z.Y. Zeng, J. Power Sources 179 (2008) 395–400.
[5] T.T. Wang, Z.H. Yang, J.H. Huang, R.J. Wang, Z.Y. Zhao, Electrochim. Acta 112 (2013) 104–110.
[6] Y.F. Yuan, J.P. Tu, H.M. Wu, Y.Z. Yang, D.Q. Shi, X.B. Zhao, Electrochim. Acta 51 (2006) 3632–3636.
[7] J. Jindra, J. Power Sources 66 (1997) 15–25.
[8] M. Geng, D.O. Northwood, Int. J. Hydrogen Energy 28 (2003) 633–636.
[9] Y.D. Cho, G.T.K. Fey, J. Power Sources 184 (2008) 610–616.
[10] R. Shivkumar, G.P. Kalaignan, T. Vasudevan, J. Power Sources 75 (1998) 90–100.
[11] Y.F. Yuan, J.P. Tu, H.M. Wu, C.Q. Zhang, S.F. Wang, X.B. Zhao, J. Power Sources 165 (2007) 905–910.
[12] D.Q. Zeng, Z.H. Yang, S.W. Wang, X. Ni, D.J. Ai, Q.Q. Zhang, Electrochim. Acta 56 (2011) 4075–4080.
[13] J. McBreen, E. Gannon, Electrochim. Acta 26 (1981) 1439–1446.
[14] Y.F. Yuan, L.Q. Yu, H.M. Wu, J.L. Yang, Y.B. Chen, S.Y. Guo, J.P. Tu, Electrochim. Acta 56 (2011) 4378–4383.
[15] J.Z. Wu, J.P. Tu, Y.F. Yuan, M. Ma, X.X. Wang, L. Zhang, R.L. Li, J. Zhang, J. Alloys Compd. 479 (2009) 624–628.
[16] J.M. Wang, L. Zhang, C. Zhang, J.Q. Zhang, J. Power Sources 102 (2001) 139–143.
[17] R. Shivkumar, G. Paruthimal Kalaignan, T. Vasudevan, J. Power Sources 55 (1995) 53–62.
[18] J.O.M. Bockris, S.U.M. Khan, Surface Electrochemistry, Plenum Press, New York, 1993, p. 904.
[19] R.J. Wen, Z.H. Yang, X.M. Fan, Z.Y. Tan, B. Yang, Electrochim. Acta 83 (2012) 376–382.
[20] Z.G. Luo, S.B. Sang, Q.M. Wu, S.Y. Liu, J. Electrochem. Soc. 2 (2012) A21–A24.
[21] K.K. Rao, M. Gravelle, J.S. Valente, F. Figueras, J. Catal. 173 (1998) 115–121.
[22] D.P. Debecker, E.M. Gaigneaux, G. Busca, Chem. A Eur. J. 15 (2009) 3920–3935.
[23] H.A. Prescott, Z.J. Li, E. Kemnitz, A. Trunschke, J. Deutsch, H. Lieske, A. Auroux, Appl. Catal. A Gen. 234 (2005) 119–130.
[24] F. Rey, V. Fornes, J.M. Rojo, Faraday Trans. 88 (1992) 2233.
[25] A.E. Palomares, J.M. Lopez-Nieto, F.J. Lazaro, A. Lopez, A. Corma, Appl. Catal. B 20 (1999) 257.
[26] I.J. Shannon, F. Rey, G. Sankar, J.M. Thomas, T. Maschmayer, A.W. Waller, A.E. Palomares, A. Corma, A.J. Dent, G.N. Greaves, Faraday Trans. 92 (1996) 4331.
[27] B. Montanari, A. Vaccari, M. Gazzano, P. Kaßner, H. Papp, R. Dziembaj, W. Makowski, T. Łojewski, Appl. Catal. B 13 (1997) 205–217.
[28] X. Fan, Z. Yang, W. Long, Z. Zhao, B. Yang, Electrochim. Acta 92 (2013) 365–370.
[29] X.M. Fan, Z.H. Yang, R.J. Wen, B. Yang, W. Long, J. Power Sources 224 (2013) 80–85.
[30] X.M. Fan, Z.H. Yang, X.E. Xie, W. Long, R.J. Wang, Z.L. Hou, J. Power Sources 241 (2013) 404–409.
[31] R.J. Wang, Z.H. Yang, RSC Adv. 3 (2013) 19924–19928.
[32] H.P. Liu, S.F. Bi, G.W. Wen, X.G. Teng, P. Gao, Z.J. Ni, Y.M. Zhu, F. Zhang, J. Alloys Compd. 543 (2012) 99–104.
[33] Y.F. Yuan, J.P. Tu, H.M. Wu, B. Zhang, X.H. Huang, X.B. Zhao, Electrochem. Commun. 8 (2006) 653–657.
[34] W. Long, Z.H. Yang, X.M. Fan, B. Yang, Z.Y. Zhao, J. Jing, Electrochim. Acta 105 (2013) 40–46.
[35] J.G. He, J.B. Wen, X.D. Li, G.W. Wang, C.H. Xu, Transactions Nonferrous Met. Soc. China 21 (2011) 1580–1586.
[36] B. Yang, Z.H. Yang, R.J. Wang, T.T. Wang, Electrochim. Acta 111 (2013) 581–587.
[37] G. Zhang, K.L. Huang, S.Q. Liu, W. Zhang, B.L. Gong, J. Alloys Compd. 426 (2006) 432–437.
[38] G. Trejo, R. Ortega, Y. Meas, P. Ozil, E. Chainet, B. Nguyen, J. Electrochem. Soc. 145 (1998) 4090–4097.